

Dual-Schedule Inversion: Training- and Tuning-Free Inversion for Real Image Editing

Jiancheng Huang* Yi Huang* Jianzhuang Liu Donghao Zhou Yifan Liu

Shifeng Chen[†]

Shenzhen Institute of Advanced Technology, Chinese Academy of Sciences

jc.huang@siat.ac.cn

Abstract

Text-conditional image editing is a practical AIGC task that has recently emerged with great commercial and academic value. For real image editing, most diffusion model-based methods use DDIM Inversion as the first stage before editing. However, DDIM Inversion often results in reconstruction failure, leading to unsatisfactory performance for downstream editing. To address this problem, we first analyze why the reconstruction via DDIM Inversion fails. We then propose a new inversion and sampling method named Dual-Schedule Inversion. We also design a classifier to adaptively combine Dual-Schedule Inversion with different editing methods for user-friendly image editing. Our work can achieve superior reconstruction and editing performance with the following advantages: 1) It can reconstruct real images perfectly without fine-tuning, and its reversibility is guaranteed mathematically. 2) The edited object/scene conforms to the semantics of the text prompt. 3) The unedited parts of the object/scene retain the original identity.

1. Introduction

The recent advancement of diffusion models [12, 13, 41, 44, 45, 49, 51, 56] has led to significant progress in text-to-image generation, and enabled a wide range of applications in AI art, film production [19, 34], and advertisement design. However, merely generating an image is often not enough. We may also want to edit an existing image using a text prompt. This task is known as text-conditional image editing [1, 8, 16–18, 21, 24, 32, 33, 39, 40, 50], which can be accomplished using pre-trained text-to-image diffusion models [3, 10, 41, 43, 52]. Due to its strong practical usage, this task has become popular and holds significant commercial value.

[†] Corresponding author. * Equal contribution.

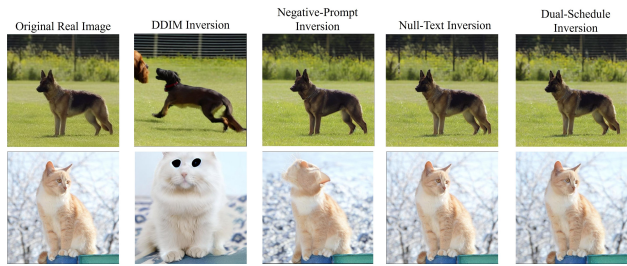


Figure 1. Examples of reconstruction by different inversion methods with guidance scale 4. While Null-Text Inversion requires fine-tuning, the other three methods do not. Dual-Schedule Inversion achieves excellent performance without fine-tuning.

Editing a synthetic image generated by a diffusion model is easier than editing a real image because the initial noisy latent $z_T \sim \mathcal{N}(0, I)$ and the sampling trajectory of this synthetic image are known [38]. For editing a real image via a diffusion model, there are mainly two types of methods, inversion-based and network-tuning-based. In the inversion-based methods [3, 10, 37, 38], the first step is usually to find its initial noisy latent z_T , which is called inversion, and then the second step is to edit it with some strategy during the sampling (generation) procedure. The network-tuning-based approaches [28, 29, 46, 54, 55] rely on training or fine-tuning the network for capturing the characteristics of the object/scene in a few images.

Many inversion-based editing methods [3, 10, 37, 38] utilize DDIM Inversion [49] for real image reconstruction. DDIM Inversion can obtain an initial noisy latent z_T from a real image I_s by inverting the sampling process, and then use this z_T as the starting point for sampling to obtain a reconstructed image \hat{I}_s . With DDIM Inversion, these methods [3, 10, 37, 38] first invert the real image into z_T , and then generate different contents by modifying the trajectory of z_t , $t \in \{T, T-1, \dots, 1\}$, during sampling. However, DDIM Inversion often fails to reconstruct the original real image [10, 37, 38] as shown in Fig. 1. Reconstruction failure makes it difficult to maintain the object/scene

consistency between the edited result and the original image. Several approaches are proposed to address this DDIM Inversion problem. The tuning-based method Null-Text Inversion [38] fine-tunes the unconditional embedding to align the sampling trajectory and the inversion trajectory as closely as possible. However, it requires the extra fine-tuning procedure. The tuning-free methods Negative-Prompt Inversion [37] and ProxEdit [9] argue that the fine-tuning in Null-Text Inversion is unnecessary, but their reconstruction and editing performances are not as good as that of Null-Text Inversion [9, 37].

Our work focuses on tuning-free inversion for real image editing without fine-tuning the network or training on a dataset. We first analyze why DDIM Inversion’s reconstruction fails mathematically, and then based on this analysis, we propose a tuning-free solution called Dual-Schedule Inversion with inversion and sampling stages. The fundamental difference from DDIM Inversion is that Dual-Schedule Inversion uses two schedules in both stages. We prove that using these two schedules guarantees that the inversion and sampling are perfectly reversible. Moreover, recognizing that different algorithms excel at different editing tasks [20, 23] (for instance, P2P [10] is good at object replacement and MasaCtrl [3] is good at action change), we develop a task classifier that seamlessly integrates our inversion approach with existing algorithms across five widely-used editing tasks. This integration aims to deliver a user-friendly experience by automatically selecting the most appropriate editing algorithm, thus enhancing editing accuracy and contextual preservation efficiently without necessitating manual algorithm selection. Our main contributions are summarized as follows.

- We mathematically analyze the reconstruction failure problem in DDIM Inversion and present the reversibility requirement.
- We propose Dual-Schedule inversion and sampling formulas to ensure the faithful reconstruction of real images, and show how to combine them with other editing methods.
- For user-friendly editing, we design a classifier to adaptively combine Dual-Schedule Inversion with different editing methods.
- Comprehensive experiments show that Dual-Schedule Inversion achieves superior reconstruction and editing performance incorporated with other editing methods.

2. Related Work

2.1. Text-to-Image Generation and Editing

With the rapid development of diffusion models, text-conditional image generation has experienced an unprecedented explosion [22, 44, 45, 47, 51, 56, 58]. Diffusion models are a kind of generative models based on nonequilibrium

thermodynamics [48], which add Gaussian noise associated with a time step to data samples (e.g., images), and train a noise estimation network to predict the noise $\epsilon \sim \mathcal{N}(0, I)$ at different time steps. At the sampling stage after training, the noise estimation network is used to gradually predict and remove the noise until a clean image is finally generated.

Diffusion models for text-conditional image generation align the feature of a textual prompt with image content by a pretrained visual language model, such as CLIP [31]. The introduction of textual prompts provides diffusion models with superior and diverse generative capabilities, such as DALL-E 3 [26], LDM [45], VQ-Diffusion [7], DALL-E 2 [44] and GLIDE [41]. On the basis of image generation, some text-conditional editing methods such as DiffEdit [5], P2P [10], InstructPix2Pix [2], PnP [52], and MasaCtrl [3] modify the sampling trajectory of an image for its editing. Besides, many subject-driven image generation methods such as Textual Inversion [6], DreamBooth [46], Custom Diffusion [29], ELITE [54], and FasterComposer [55] can generate different new images of the same subject according to the given subject images, which can also be treated as image editing methods.

2.2. Diffusion Model Inversion

Diffusion inversion is to reverse the sampling process, which sequentially corrupts a sample with predicted noises [49]. For real image editing, existing methods mostly utilize DDIM Inversion [49], which is designed to obtain a deterministic noisy latent z_T from a real image z_0 , and then uses this z_T as the starting point of the sampling process to modify the trajectory such that a new image is obtained.

However, as mentioned in Sec. 1, reconstruction failure is common in DDIM Inversion, which causes the identity of the unedited parts not to be maintained. In order to solve this problem, some methods [6, 38, 46] choose to fine-tune certain parameters. For instance, Null-Text Inversion [38] aligns inversion and sampling trajectories by fine-tuning the unconditional embedding. Negative-Prompt Inversion [37] and ProxEdit [9] argue that the fine-tuning in Null-Text Inversion [38] is unnecessary and present their tuning-free methods for reconstruction. However, the performances of Negative-Prompt Inversion and ProxEdit are not as good as Null-Text Inversion [9, 37]. Besides, these methods [9, 37, 38] occupy the negative prompt [14] position for reconstruction, making negative prompts unusable.

Some recent works propose to modify the inversion and sampling formula. For instance, EDICT [53] uses affine coupling layers as its inversion and sampling steps. However, [53] introduces substantial modifications to the sampling formula, which may complicate its integration with other image editing techniques. DDPM Inversion [25] introduces a DDPM latent noise space for more diversity.

Our Dual-Schedule Inversion, on the other hand, emphasizes achieving high-quality image reconstruction by making slight modifications to DDIM inversion and sampling. Thus, editing methods designed for DDIM can also be integrated with our inversion. Moreover, our method’s compatibility with various editing techniques makes it adaptable to different editing tasks.

In Table S8 of our supplementary material, we summarize recent inversion and editing methods. Our Dual-Schedule Inversion is training- and tuning-free, does not occupy the negative prompt position, and is mathematically reversible.

3. Background

Diffusion Model Training. The training of a diffusion model starts with a clean sample z_0 , and a diffusion process is carried out by adding Gaussian noise to z_0 as $q(z_t|z_0) = \mathcal{N}(\sqrt{\alpha_t}z_0, (1 - \alpha_t)I)$, where α_t is a predefined diffusion schedule, $t \in \{1, 2, \dots, T\}$ is the time-step, z_t is the noisy latent, and $z_T \sim \mathcal{N}(0, I)$. In DDPM [12], the common setting of T is 1000. The optimization of the diffusion model is simplified to train a network $\epsilon_\theta(z_t, t)$ that predicts the Gaussian noise $\epsilon \sim \mathcal{N}(0, I)$ with this loss:

$$L_{simple} = \mathbb{E}_{z_0, t, \epsilon} \left[\|\epsilon - \epsilon_\theta(z_t, t)\|^2 \right].$$

DDIM Sampling and Inversion. Given a real image z_0 , common editing methods [3, 35, 38] first invert this z_0 to a z_T by some inversion scheme. Then, they start the sampling process from this z_T and use their editing strategies to generate an edited result \tilde{z}_0 . Ideally, direct sampling from this z_T without any editing should reconstruct a \tilde{z}_0 that is as close to z_0 as possible. If this \tilde{z}_0 is very different from z_0 , called reconstruction failure, the corresponding edited image cannot retain the identity of the unedited parts in z_0 . Therefore, an inversion method that satisfies $\tilde{z}_0 \approx z_0$ is desired.

We first analyze the commonly used DDIM sampling and inversion, whose sampling equation is as follows:

$$z_{t-1} = \sqrt{\alpha_{t-1}} \frac{z_t - \sqrt{1 - \alpha_t} \epsilon_\theta(z_t, t)}{\sqrt{\alpha_t}} + \sqrt{1 - \alpha_{t-1}} \epsilon_\theta(z_t, t), \quad (1)$$

which can be rewritten as:

$$z_t = \sqrt{\alpha_t} \frac{z_{t-1} - \sqrt{1 - \alpha_{t-1}} \epsilon_\theta(z_t, t)}{\sqrt{\alpha_{t-1}}} + \sqrt{1 - \alpha_t} \epsilon_\theta(z_t, t). \quad (2)$$

Eq. 2 seems to be used as a perfect inversion from z_{t-1} to z_t . However, the problem is that z_t is unknown and used as the input to the network $\epsilon_\theta(z_t, t)$. Thus, DDIM Inversion [49] and several methods [15, 42, 53] assume that $z_{t-1} \approx z_t$, and replace z_t on the right hand side of Eq. 2 with z_{t-1} , resulting in the following approximation:

$$z_t = \sqrt{\alpha_t} \frac{z_{t-1} - \sqrt{1 - \alpha_{t-1}} \epsilon_\theta(z_{t-1}, t)}{\sqrt{\alpha_{t-1}}} + \sqrt{1 - \alpha_t} \epsilon_\theta(z_{t-1}, t). \quad (3)$$

Text Condition and Classifier-Free Guidance. Text-conditional diffusion models aim to generate a result from a random noise z_T with a text prompt P . During the sampling process at inference, the noise estimation network $\epsilon_\theta(z_t, t, C)$ is used to predict the noise ϵ , where $C = \psi(P)$ is the text embedding. The noise in z_t is gradually removed for T steps until z_0 is obtained.

In text-conditional image generation, it is necessary to give enough textual control and influence over the generation. Ho et al. [14] propose classifier-free guidance where conditional and unconditional predictions are combined. Specifically, let $\emptyset = \psi(\text{“”})$ ¹ be the null text embedding and w be the guidance scale. Then the classifier-free guidance prediction is defined by:

$$\epsilon_\theta(z_t, t, C, \emptyset) = w \epsilon_\theta(z_t, t, C) + (1 - w) \epsilon_\theta(z_t, t, \emptyset), \quad (4)$$

where $\epsilon_\theta(z_t, t, C, \emptyset)$ is used to replace $\epsilon_\theta(z_t, t)$ in the sampling Eq. 1, and w is usually in [1, 7.5] [45, 47]. The higher w means the stronger control by the text.

Image Editing. Given a real image I_s and a related text prompt P_s , the goal is to generate a new image I_t with the target prompt P_t using a pretrained diffusion model such that I_t aligns with P_t . This task is challenging, particularly on real images, as most image editing methods struggle to edit real images while preserving good reconstruction performance [10, 38, 52]. A popular way used by many editing methods [3, 10, 37, 52] is: 1) using DDIM Inversion on the original image I_s to get its z_T , and 2) using P_t and this z_T as the starting point to generate I_t . However, as shown in Fig. 1, DDIM Inversion often fails to reconstruct the original image, making the identity of the object/scene in I_t changed.

4. Method

We first analyze why the reconstruction of a real image via DDIM Inversion fails in Sec. 4.1. Then, in Sec. 4.2, we propose our Dual-Schedule Inversion for inversion and sampling, and show that it mathematically guarantees perfect reconstruction. Finally, we introduce five categories of editing tasks and our task classifier that integrates our inversion approach with existing editing methods.

4.1. Irreversibility of DDIM Inversion

In DDIM sampling [49], to speed up the time-consuming sampling procedure, $[t_0, t_0 + s, t_0 + 2s, \dots, t_0 + T's]$, instead of $[1, 2, \dots, T]$, is chosen where s is the interval and $T' < T$. For example, if $t_0 = 1$, $s = 20$, and $T' = 50$, then the schedule is $[1, 21, 41, \dots, 961, 981]$; if $t_0 = 10$, $s = 20$, and $T' = 50$, then the schedule is $[10, 30, 50, \dots, 990]$. In the rest of this paper, as shown in Fig. 2, we use $[t_0, t_0 +$

¹The position for \emptyset is often used by negative prompts such that some attributes do not appear in the generated image.

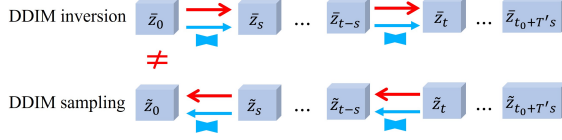


Figure 2. DDIM Inversion is irreversible.

$s, \dots, t_0 + T's]$ to denote the sampling schedule, and thus the noisy latents during sampling are $\tilde{z}_{t_0+T's}, \dots, \tilde{z}_{t_0+s}, \tilde{z}_{t_0}$. In this case, Eq. 1 is rewritten as:

$$\tilde{z}_{t-s} = a_{(t \rightarrow t-s)} \tilde{z}_t + b_{(t \rightarrow t-s)} \epsilon_{\theta}(\tilde{z}_t, t), \quad (5a)$$

$$\begin{aligned} a_{(t \rightarrow t-s)} &= \sqrt{\alpha_{t-s}/\alpha_t}, \\ b_{(t \rightarrow t-s)} &= \sqrt{1 - \alpha_{t-s}} - \frac{\sqrt{1 - \alpha_t} \sqrt{\alpha_{t-s}}}{\sqrt{\alpha_t}}, \end{aligned} \quad (5b)$$

where $b_{(t \rightarrow t-s)}$ and $a_{(t \rightarrow t-s)}$ are constant coefficients from t to $t-s$. Besides, we use $\tilde{z}_{t_0}, \tilde{z}_{t_0+s}, \dots, \tilde{z}_{t_0+T's}$ to denote the noisy latents during inversion. Again, we rewrite the approximation Eq. 3 (DDIM inversion) as:

$$\tilde{z}_t = a_{(t-s \rightarrow t)} \tilde{z}_{t-s} + b_{(t-s \rightarrow t)} \epsilon_{\theta}(\tilde{z}_{t-s}, t), \quad (6a)$$

$$\begin{aligned} a_{(t-s \rightarrow t)} &= \sqrt{\alpha_t/\alpha_{t-s}}, \\ b_{(t-s \rightarrow t)} &= \sqrt{1 - \alpha_t} - \frac{\sqrt{1 - \alpha_{t-s}} \sqrt{\alpha_t}}{\sqrt{\alpha_{t-s}}}, \end{aligned} \quad (6b)$$

where $a_{(t-s \rightarrow t)}$ and $b_{(t-s \rightarrow t)}$ are another two constant coefficients from $t-s$ to t . Furthermore, Eq. 6a can be derived as:

$$\tilde{z}_{t-s} = a_{(t \rightarrow t-s)} \tilde{z}_t + b_{(t \rightarrow t-s)} \epsilon_{\theta}(\tilde{z}_{t-s}, t). \quad (7)$$

Comparing Eq. 5a and Eq. 7, if we want to have the exact inversion $\tilde{z}_{t-s} = \tilde{z}_{t-s}$, it is necessary that $\tilde{z}_t = \tilde{z}_t$ and $\tilde{z}_t = \tilde{z}_{t-s}$, which lead to $\tilde{z}_{t_0+T's} = \tilde{z}_0$, meaning that there is no any diffusion. Therefore, DDIM Inversion is mathematically irreversible. In the next section, we propose a solution.

4.2. Dual-Schedule Inversion

Reversibility Requirement. Based on Eq. 5a and Eq. 6a, we define the following sampling and inversion formulas:

$$\tilde{z}_{t-s} = a_{(t \rightarrow t-s)} \tilde{z}_t + b_{(t \rightarrow t-s)} \epsilon_{\theta}(\tilde{z}_t, \tau), \quad (8)$$

$$\tilde{z}_t = a_{(t-s \rightarrow t)} \tilde{z}_{t-s} + b_{(t-s \rightarrow t)} \epsilon_{\theta}(\tilde{z}_{t-s}, \tau), \quad (9)$$

where $a_{(t \rightarrow t-s)}$, $b_{(t \rightarrow t-s)}$, $a_{(t-s \rightarrow t)}$ and $b_{(t-s \rightarrow t)}$ are computed via Eq. 5b and Eq. 6b. We call \tilde{z}_{τ} and \tilde{z}_{τ} satisfying $\tilde{z}_{\tau} = \tilde{z}_{\tau}$ the *auxiliary latents*.

Similar to Eq. 7, Eq. 9 can be rewritten as:

$$\tilde{z}_{t-s} = a_{(t \rightarrow t-s)} \tilde{z}_t + b_{(t \rightarrow t-s)} \epsilon_{\theta}(\tilde{z}_{\tau}, \tau). \quad (10)$$

Comparing Eq. 8 and Eq. 10, we can see that $\tilde{z}_{t-s} = \tilde{z}_{t-s}$ as long as $\tilde{z}_t = \tilde{z}_t$. Therefore, satisfying $\tilde{z}_{\tau} = \tilde{z}_{\tau}$ and

$\tilde{z}_t = \tilde{z}_t$ guarantees the perfect reversibility ($\tilde{z}_{t-s} = \tilde{z}_{t-s}$) in Eq. 8 and Eq. 9. Since $\tilde{z}_{t_0+T's} = \tilde{z}_{t_0+T's}$, now the problem becomes how to find \tilde{z}_{τ} and \tilde{z}_{τ} such that $\tilde{z}_{\tau} = \tilde{z}_{\tau}$.

Primary and Auxiliary Schedules. To obtain the auxiliary latents, we design two schedules, as shown in Fig. 3(a), where the upper and lower parts are called the *primary schedule* and the *auxiliary schedule*, respectively.

The primary time schedule is, e.g., $[1, 21, 41, \dots, 981]$ with $T' = 50$. In these 50 steps, we use $\{z_t^p\}$ to denote the *primary latents* $[z_1^p, z_{21}^p, z_{41}^p, \dots, z_{981}^p]$. Given these time-steps of the primary schedule, we also design an auxiliary schedule $[10, 30, 50, \dots, 970]$. This auxiliary schedule is for obtaining the auxiliary latents $z_{\tau} = \tilde{z}_{\tau} = \tilde{z}_{\tau}$, where $\tau \in \{10, 30, 50, \dots, 970\}$. For example, between time-steps 21 and 41 in the primary schedule, τ is chosen as the midpoint 30. We use $\{z_t^a\}$ to denote the auxiliary latents $[z_{10}^a, z_{30}^a, z_{50}^a, \dots, z_{970}^a]$.

Dual-Schedule Inversion. As shown in Fig. 3(a), we design the iterative inversion of the primary schedule as follows where \tilde{z}_t^p and \tilde{z}_t^a denote the latents during inversion:

$$\tilde{z}_t^p = a_{(t-20 \rightarrow t)} \tilde{z}_{t-20}^p + b_{(t-20 \rightarrow t)} \epsilon_{\theta}(\tilde{z}_{t-11}^a, t-11), \quad (11)$$

where $t = [21, \dots, 961, 981]$. Eq. 11 is one implementation of Eq. 9 and \tilde{z}_{t-11}^a is the auxiliary latent from \tilde{z}_{t-20}^p to \tilde{z}_t^p .

Also, for the iterative inversion of the auxiliary schedule, we have the inversion formula:

$$\tilde{z}_t^a = a_{(t-20 \rightarrow t)} \tilde{z}_{t-20}^a + b_{(t-20 \rightarrow t)} \epsilon_{\theta}(\tilde{z}_{t-9}^p, t-9), \quad (12)$$

where $t = [30, \dots, 950, 970]$. In Eq. 11 and Eq. 12, \tilde{z}_{10}^p and \tilde{z}_{10}^a are obtained by the original process of DDIM since they are the starting of the schedule. This calculation does not affect our reversibility, which is proved in the supplementary material.

Dual-Schedule Sampling. To reconstruct I_s perfectly, as shown in Fig. 3(b), we devise a sampling formula Eq. 13 for the primary schedule, where \tilde{z}_t^p and \tilde{z}_t^a denote the latents during sampling:

$$\tilde{z}_{t-20}^p = a_{(t \rightarrow t-20)} \tilde{z}_t^p + b_{(t \rightarrow t-20)} \epsilon_{\theta}(\tilde{z}_{t-11}^a, t-11), \quad (13)$$

where $t = [981, 961, \dots, 21]$. Eq. 13 is one implementation of Eq. 8. Comparing Eq. 13 and Eq. 11 with Eq. 8 and Eq. 9, since $\tilde{z}_{t_0+T's}^p = \tilde{z}_{t_0+T's}^p$, it is obvious that we can guarantee $\tilde{z}_{t-20}^p = \tilde{z}_{t-20}^p$ as long as $\tilde{z}_{t-11}^a = \tilde{z}_{t-11}^a$. For obtaining $\tilde{z}_{t-11}^a = \tilde{z}_{t-11}^a$, given $\tilde{z}_{t_0+T's}^a = \tilde{z}_{t_0+T's}^a$, we design the sampling formula for the auxiliary schedule:

$$\tilde{z}_{t-20}^a = a_{(t \rightarrow t-20)} \tilde{z}_t^a + b_{(t \rightarrow t-20)} \epsilon_{\theta}(\tilde{z}_{t-9}^p, t-9), \quad (14)$$

where $t = [970, 950, \dots, 30]$. Eq. 12 and Eq. 14 are also one implementation of Eq. 9 and Eq. 8, respectively.

Reversibility. As stated in the beginning of this section, the reversibility requirement is $\tilde{z}_{\tau} = \tilde{z}_{\tau}$ and $\tilde{z}_t = \tilde{z}_t$.

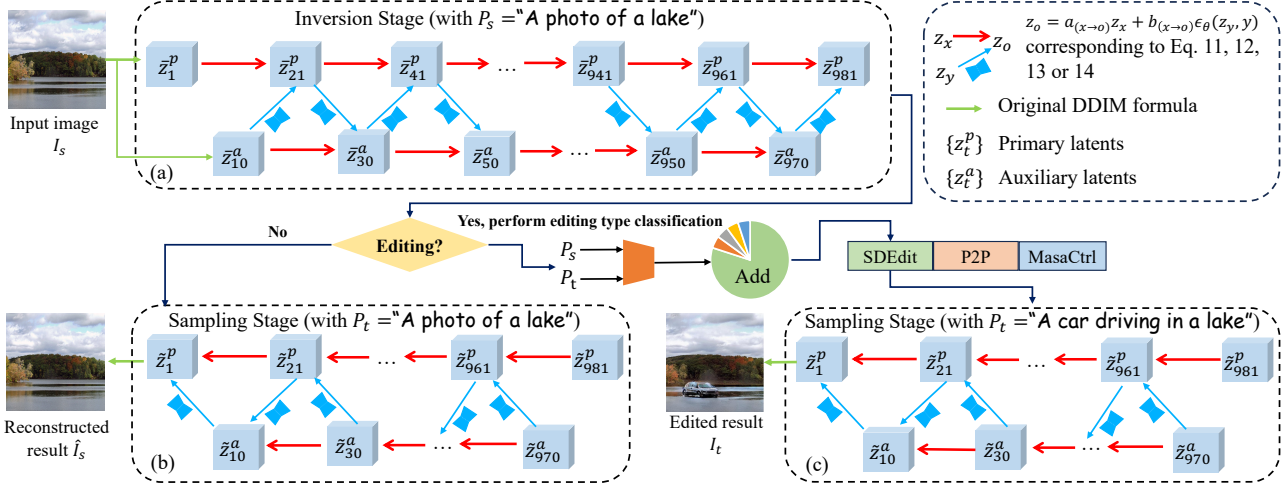


Figure 3. Pipeline of Dual-Schedule Inversion, which is divided into inversion and sampling stages. The inversion stage (a) is for getting \tilde{z}_{981}^p and \tilde{z}_{970}^a . The sampling stage is used for reconstruction (b) or editing (c) depending on the target prompt. Both stages have two time schedules where two specific schedules [1, 21, 41, ..., 981] and [10, 30, 50, ..., 970] are used for example.

Given $\tilde{z}_{981}^p = \tilde{z}_{981}^p$ and $\tilde{z}_{970}^a = \tilde{z}_{970}^a$, we have $\tilde{z}_{961}^p = \tilde{z}_{961}^p$ according to Eq. 11 and Eq. 13. Then, given $\tilde{z}_{961}^p = \tilde{z}_{961}^p$ and $\tilde{z}_{970}^a = \tilde{z}_{970}^a$, we have $\tilde{z}_{950}^a = \tilde{z}_{950}^a$ according to Eq. 12 and Eq. 14. Repeating this process, our Dual-Schedule Inversion can finally guarantee perfect reversibility $\tilde{z}_1^p = \tilde{z}_1^p$, as illustrated in Fig. 3 (a) and (b).

4.3. Dual-Schedule Inversion for Editing

After the above design of the Dual-Schedule Inversion for reconstruction, it can be easily combined with common editing methods for editing. For example, a direct editing way is to use a different target prompt in Dual-Schedule Inversion’s sampling (see Fig. 3(c)). We can also replace DDIM Inversion with Dual-Schedule Inversion in the recent editing methods [3, 10, 35].

Five Categories of Editing Tasks. We classify text-conditional image editing into five categories: 1) *Object Replacement*: Replacing an object in the image with another object; 2) *Action Editing*: Preserving the background and the object identity but altering his/her/its action; 3) *Scene Editing*: Keeping the objects in the image unchanged while transforming the scene; 4) *New Object Creation*: Adding a new object to the image while keeping the unedited part of the image unchanged; 5) *Style Editing*: Modifying the artistic style of the image. Our Dual-Schedule Inversion is a universal inversion method that can be adapted to all these editing categories by combining it with other image editing techniques, such as SDEdit [35], P2P [10], and MasaCtrl [3].

Automatic Determination of Editing Tasks based on Descriptions. Given the diverse requirements of the five editing tasks, it is imperative to tailor distinct editing methods to different tasks, because different methods are good at different tasks. For the object replacement and scene edit-

ing tasks, we combine our Dual-Schedule Inversion with P2P [10]; for the action editing task, we combine it with MasaCtrl [3]; for new object adding and style editing, we combine it with SDEdit [35]. However, making users identify editing types and choose algorithms is overly complex. To automate and seamlessly cater to users’ needs across various editing tasks, we propose an approach capable of automatically determining the editing task.

Specifically, with in-context learning [36], we first utilize GPT-4 to generate a substantial dataset of triple samples, each comprising a source text, a target text, and an associated editing task label. Subsequently, leveraging the text embeddings extracted by the CLIP text encoder, we design a Transformer-based editing task classifier as shown in Fig. 3. This classifier takes as input the concatenated embeddings of the source and target texts. After processing through multiple Transformer blocks, a classification head at the final layer outputs the predicted editing task category.

With this task classifier that is trained on the dataset, the editing process becomes significantly more user-friendly. The user is required to input an image. We first employ BLIP [30] to generate a caption, providing a source text description. The user then inputs a desired target text. Our task classifier, receiving both the source and target texts as input, predicts the corresponding editing task type (one of the five categories). Based on this classification, our system dynamically selects the appropriate editing method for our Dual-Schedule Inversion, simplifying user interaction and enhancing the editing outcome by automatically adapting the strategy to match the identified task.

5. Experiments

We evaluate Dual-Schedule Inversion’s performances of reconstruction in Sec. 5.1 and editing in Sec. 5.2 on real im-

Method		Structure	Background Preservation				CLIP Similariy	
Inversion	Editing	Distance $\times 10^3$ ↓	PSNR ↑	LPIPS $\times 10^3$ ↓	MSE $\times 10^4$ ↓	SSIM $\times 10^2$ ↑	Whole ↑	Edited ↑
AIDI	P2P	39.33	22.84	89.50	52.2	71.38	23.50	20.31
NMG	P2P	14.15	26.02	42.32	24.9	76.84	25.17	22.90
EDICT	P2P	15.20	26.30	39.49	23.4	78.50	24.62	21.87
ProxEdit	P2P	13.70	24.35	69.58	36.9	73.40	23.80	21.70
DirectInv	P2P	14.56	26.10	46.50	24.5	77.30	26.70	23.84
DDIM	P2P	68.70	20.72	102.97	84.6	66.40	23.80	20.07
Ours	P2P	13.09	26.35	39.50	23.3	<u>78.12</u>	27.50	<u>23.00</u>

Table 1. Comparison with SOTA inversion methods on editing.

Method	Tuning-free	PSNR ↑	SSIM ↑
DDIM Inversion	✓	16.348	0.509
Negative-Prompt Inversion	✓	21.352	0.624
Null-Text Inversion	✗	26.106	0.738
Dual-Schedule Inversion	✓	25.977	0.738
Upper Bound		26.310	0.742

Table 2. Reconstruction performance. The values are computed on the testing dataset with three guidance scales.

ages using the pre-trained popular Stable Diffusion model [45]. Due to the lack of public benchmarks for this evaluation, we build a testing set in this work. The set has a total of 150 image-text pairs, among which 32 pairs are from all the examples used by three related works^{1,2,3} [2, 3, 54], and the rest of 118 pairs are from the Internet. It includes images of animals, humans, man-made objects, and scenes, some of which are of low quality or contain complex textures, increasing the possibility of distortion in reconstruction. All images are interpolated, cut, and/or scaled to the size of 512×512. All the image-text pairs are listed in the supplementary material. For the implementation of our Dual-Schedule Inversion, the primary schedule is [1, 21, 41, ..., 961, 981] and the auxiliary schedule is [10, 30, 50, ..., 990].

5.1. Reconstruction Performance

In the reconstruction experiment, we compare Dual-Schedule Inversion with three recent inversion methods, DDIM Inversion [49] (baseline), Null-Text Inversion [38], and Negative-Prompt Inversion [37], under different guidance scales w in Eq. 4. To ensure an unbiased comparison, all experiments are conducted with fair sampling steps. Specifically, we maintain identical sampling times by using 50 steps for each of our two schedules and 100 steps for other methods. The quantitative comparison is presented in Table 2, and two qualitative examples are in Fig. 1 (more examples are provided in the supplementary material). We calculate the average PSNR and SSIM on this testing set

across three different guidance scales 1.0, 4.0, and 7.5.

In Fig. 1, we clearly see that DDIM Inversion leads to obvious reconstruction failures. Most of its reconstructed images are very different from the source images, and its PSNR and SSIM values are far below those of the other methods (Table 2). Thus, editing real images using this baseline can lead to severe distortions, including object/scene identity distortions (see Sec. 5.2). Our Dual-Schedule Inversion significantly outperforms Negative-Prompt Inversion quantitatively. Compared with Null-Text Inversion, our method has the same SSIM, with a slightly lower PSNR (25.977 vs. 26.106). However, Null-Text Inversion requires an extra fine-tuning stage.

In Table 2, we also show the upper bound for the reconstruction quality. Stable Diffusion model uses an encoder to encode an image to a latent space, in which sampling is performed, and uses a decoder to decode the final latent into the image space. So the upper bound is obtained without the sampling stage. We can see that the results of Dual-Schedule Inversion and Null-Text Inversion are close to the upper bound. Though our method is mathematically reversible, the small gap between it and the upper bound comes from the numerical errors during sampling.

To demonstrate the robustness and efficacy of our inversion method during editing, compared to other SOTA inversion techniques, we adopt the metrics from [27] to evaluate reconstruction ability during editing on 20 real images. Specifically, the structure distance and background preservation metrics in Table 1 represent the reconstruction performance of the unedited parts. Structure distance computes the distance between structure features extracted from DINO-ViT. For background preservation, [27] computes PSNR, LPIPS, MSE, and SSIM in the unedited area with manual-annotated masks. Following [27], we also obtain these masks on the source image in the same way. We uniformly equip the six inversion methods and ours with the same editing technique (P2P) to test their effectiveness. As shown in Table 1, our inversion method overall achieves the best performance. To explore the performance improvements of our inversion across different editing techniques, we conduct experiments on three editing methods. As shown in Table 3, the results demonstrate that our inversion method enhances all these editing techniques.

¹timothybrooks.com/instruct-pix2pix

²https://ljzycmd.github.io/projects/MasaCtrl

³https://github.com/csyxwei/ELITE

Method		Structure	Background Preservation				CLIP Simiary	
Inversion	Editing	Distance $\times 10^3$ ↓	PSNR ↑	LPIPS $\times 10^3$ ↓	MSE $\times 10^4$ ↓	SSIM $\times 10^2$ ↑	Whole ↑	Edited ↑
DDIM	P2P	68.70	20.72	102.97	84.6	66.40	23.80	20.07
Ours	P2P	13.09	26.35	39.50	23.3	78.12	27.50	23.00
DDIM	MasaCtrl	70.80	21.26	97.54	74.1	69.27	21.92	20.38
Ours	MasaCtrl	13.95	25.96	43.50	25.4	77.50	23.20	21.50
DDIM	SDEdit	75.70	18.85	117.53	130.3	64.83	22.18	20.95
Ours	SDEdit	14.60	25.65	47.51	27.2	76.50	24.05	21.78

Table 3. Performance improvements of three editing methods using our inversion technique.

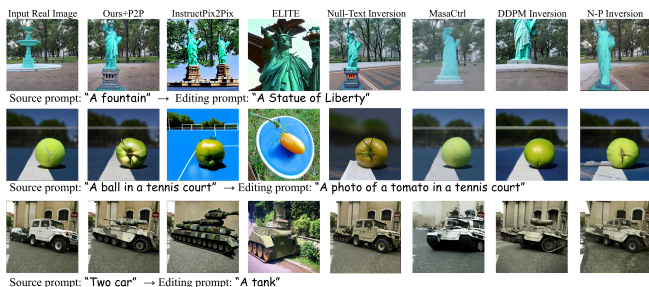


Figure 4. Comparison with SOTA editing methods on real images for *Object Replacement*. N-P Inversion denotes Negative-Prompt Inversion.



Figure 5. Comparison with SOTA editing methods on real images for *Action Editing*.

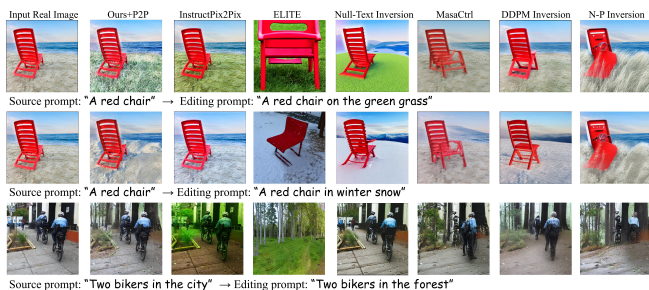


Figure 6. Comparison with SOTA editing methods on real images for *Scene Editing*.

5.2. Editing Performance

We compare with seven SOTA editing methods: InstructPix2Pix [2], MasaCtrl [3], ELITE [54], DDPM Inversion [25], DreamBooth [46], Negative-Prompt Inversion [37], and Null-Text Inversion [38]. The visual comparisons for the five editing categories are shown in Figs. 4–8, respectively. Most of the compared methods fail to solve the following two problems simultaneously: 1) the unedited



Figure 7. Comparison with SOTA editing methods on real images for *Object Adding*.

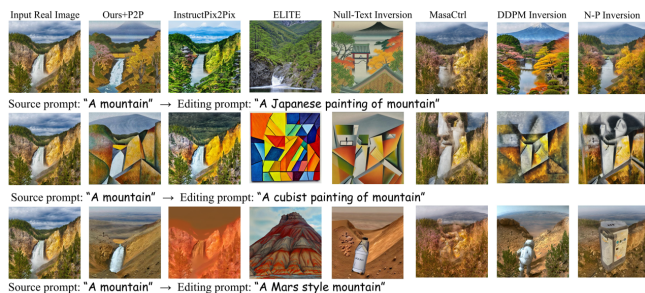


Figure 8. Comparison with SOTA editing methods on real images for *Style Editing*.

Method	Null-Text Inversion	DreamBooth	ELITE	N-P Inversion
User Score ↑	5.15	2.89	1.95	1.77
CLIP Score ↑	0.2819	0.2599	0.2509	0.3031
LPIPS ↓	0.035	0.1663	0.1545	0.0866

Method	InstructPix2Pix	MasaCtrl	DDPM Inversion	Ours
User Score ↑	4.99	4.15	5.48	5.85
CLIP Score ↑	0.2401	0.2529	0.2614	0.3041
LPIPS ↓	0.097	0.0778	0.0715	0.018

Table 4. Quantitative results of different editing methods. The user scores are in the range of [0, 10]. N-P Inversion denotes Negative-Prompt Inversion.

part of an image cannot retain its original identity; 2) the edited results do not match the editing prompts. Specifically, ELITE, MasaCtrl, DDPM Inversion, and Negative-Prompt Inversion often result in identity distortions. InstructPix2Pix and Null-Text Inversion tend to retain the structure of the object, so they are not able to perform action editing. MasaCtrl [3] is designed for action editing and it is not able to perform object or scene replacement. Our method is able to solve these two problems simultaneously in various types of editing because of its perfect reconstruct-

Method		Structure	Background Preservation				CLIP Similarity	
Inversion	Editing	Distance $\times 10^3$ ↓	PSNR ↑	LPIPS $\times 10^3$ ↓	MSE $\times 10^4$ ↓	SSIM $\times 10^2$ ↑	Whole ↑	Edited ↑
Ours	P2P	13.09	26.35	39.50	23.3	78.12	27.50	23.00
Ours	MasaCtrl	13.95	25.96	43.50	25.4	77.50	23.20	21.50
Ours	SDEdit	14.60	25.65	47.51	27.2	76.50	24.05	21.78
Ours	Classifier	12.98	26.42	38.17	22.80	78.93	30.41	25.43

Table 5. Ablation study for our classifier.

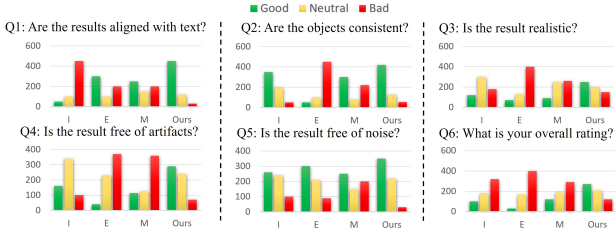


Figure 9. Comparison with three most recent SOTA methods for 6 specific questions with 3 possible answers (good, neutral, bad), where I, E, and M denote InstructPix2Pix, ELITE, and MasaCtrl, respectively.

tion capability.

For quantitative evaluation, since there is no image editing benchmark, similar to [54], we conduct a user study with 30 participants to evaluate 180 edited results by the 8 methods on 20 real images. The participants are asked to score the overall editing quality of these results from 1 (worst) to 10 (best), based on the following two criterions: 1) consistency of the results with the original image, and 2) consistency of the results with the editing prompt. For each image, 8 edited results by the methods are shown to each participant. The average user scores, CLIP Score [11], and LPIPS [57] are reported in Table 4, where our method obtains the best scores (see DiffEdit [5] about how to calculate CLIP Score and LPIPS). In order to analyze the detailed aspects influencing these scores, we specifically design 6 Q&As and compare with 3 most recent methods, Instruct-Pix2Pix [2], MasaCtrl [3], and ELITE [54]. Fig. 9 reports the rating distributions of the 4 methods, among which ours receives more “good” and fewer “bad” answers.

5.3. Ablation Study

Auxiliary Schedules. In Fig. 3 and the reconstruction experiments, the primary schedule is $[1, 21, 41, \dots, 961, 981]$ and the auxiliary schedule is $[10, 30, 50, \dots, 950, 970]$, where $\tau = t - s + \frac{s}{2}$ (see Eq. 8 and Eq. 9). In fact, τ can be set to other values such as $\tau = t - s + \frac{1}{4}s$ and $\tau = t - s + \frac{3}{4}s$. From the second column in Table 6, we can see that the reconstruction performances are very similar in these three settings of τ . However, we find that when $\tau = t - s + \frac{1}{4}s$ or $\tau = t - s + \frac{3}{4}s$, the editing performances are not as good as when $\tau = t - s + \frac{s}{2}$ (see the supplementary material). We suspect that when $\tau = t - s + \frac{s}{2}$ (i.e., the

T'	50	50	50	50	20
τ	$t - s + \frac{1}{4}s$	$t - s + \frac{3}{4}s$	$t - s + \frac{s}{2}$	$t - s + \frac{s}{2}$	$t - s + \frac{s}{2}$
PSNR ↑	25.961	25.963	25.977	25.977	25.945
SSIM ↑	0.737	0.737	0.738	0.738	0.732

Table 6. Ablation Study for τ and T' .

midpoint between $t - s$ and t), the auxiliary latent \tilde{z}_τ^a can better balance the sampled primary latents \tilde{z}_{t-s}^p and \tilde{z}_t^a .

Schedule Lengths. In Fig. 3 and all the editing examples, the numbers of the sampling steps are all 50 ($T' = 50$, defined in Sec. 4.1). Our Dual-Schedule Inversion can be applied to fewer or more steps. In the third column of Table 6, we compare its reconstruction performances when $T' = 50$ and $T' = 20$, and see that the performance drops only slightly when $T' = 20$, showing that it is robust to different sampling steps.

Task Classifier. To further demonstrate the efficacy of the task classifier within our pipeline, we integrate our Dual-Schedule Inversion framework with SDEdit, P2P, and MasaCtrl, both with and without the implementation of the task classifier. This evaluation is carried out on our testing set comprising 150 images, distributed across the five editing tasks. The results are detailed in Table 5, which reveals a notable drop in editing performance when the task classifier is not utilized due to the fact that each algorithm is only good at specific tasks. By adaptively selecting the most appropriate algorithm for each specific task, our inversion approach facilitates a more user-friendly application.

6. Conclusion and Limitation

In this paper, we propose a tuning-free Dual-Schedule Inversion that enables faithful reconstruction and editing on real images. With the novel design of the primary and auxiliary schedules for inversion and sampling, our method guarantees reversibility mathematically. Combining it with other editing techniques, it achieves SOTA editing performance on object replacement, action editing, scene editing, new object creation, and style editing.

Since it needs to be integrated with other editing techniques for image editing, its editing ability is restricted by these techniques. When a more powerful editing method appears, its editing competence will also be boosted.

References

- [1] Manuel Brack, Felix Friedrich, Katharia Kornmeier, Linoy Tsaban, Patrick Schramowski, Kristian Kersting, and Apolinário Passos. Ledits++: Limitless image editing using text-to-image models. In *CVPR*, pages 8861–8870, 2024. [1](#)
- [2] Tim Brooks, Aleksander Holynski, and Alexei A Efros. Instructpix2pix: Learning to follow image editing instructions. In *CVPR*, 2023. [2](#), [6](#), [7](#), [8](#)
- [3] Mingdeng Cao, Xintao Wang, Zhongang Qi, Ying Shan, Xiaohu Qie, and Yinqiang Zheng. Masactrl: Tuning-free mutual self-attention control for consistent image synthesis and editing. In *ICCV*, 2023. [1](#), [2](#), [3](#), [5](#), [6](#), [7](#), [8](#)
- [4] Hansam Cho, Jonghyun Lee, Seoung Bum Kim, Tae-Hyun Oh, and Yonghyun Jeong. Noise map guidance: Inversion with spatial context for real image editing. In *ICLR*, 2024. [2](#)
- [5] Guillaume Couairon, Jakob Verbeek, Holger Schwenk, and Matthieu Cord. Diffedit: Diffusion-based semantic image editing with mask guidance. *ICLR*, 2023. [2](#), [8](#)
- [6] Rinon Gal, Yuval Alaluf, Yuval Atzmon, Or Patashnik, Amit H Bermano, Gal Chechik, and Daniel Cohen-Or. An image is worth one word: Personalizing text-to-image generation using textual inversion. In *ICLR*, 2023. [2](#)
- [7] Shuyang Gu, Dong Chen, Jianmin Bao, Fang Wen, Bo Zhang, Dongdong Chen, Lu Yuan, and Baining Guo. Vector quantized diffusion model for text-to-image synthesis. In *CVPR*, 2022. [2](#)
- [8] Qin Guo and Tianwei Lin. Focus on your instruction: Fine-grained and multi-instruction image editing by attention modulation. In *CVPR*, pages 6986–6996, 2024. [1](#)
- [9] Ligong Han, Song Wen, Qi Chen, Zhixing Zhang, Kunpeng Song, Mengwei Ren, Ruijiang Gao, Yuxiao Chen, Di Liu, Qilong Zhangli, et al. Proxedit: Improving tuning-free real image editing with proximal guidance. *WACV*, 2024. [2](#)
- [10] Amir Hertz, Ron Mokady, Jay Tenenbaum, Kfir Aberman, Yael Pritch, and Daniel Cohen-Or. Prompt-to-prompt image editing with cross attention control. In *ICLR*, 2023. [1](#), [2](#), [3](#), [5](#)
- [11] Jack Hessel, Ari Holtzman, Maxwell Forbes, Ronan Le Bras, and Yejin Choi. Clipscore: A reference-free evaluation metric for image captioning. In *EMNLP*, pages 7514–7528, 2021. [8](#)
- [12] Jonathan Ho, Ajay Jain, and Pieter Abbeel. Denoising diffusion probabilistic models. In *NeurIPS*, 2020. [1](#), [3](#)
- [13] Jonathan Ho, Chitwan Saharia, William Chan, David J Fleet, Mohammad Norouzi, and Tim Salimans. Cascaded diffusion models for high fidelity image generation. *The Journal of Machine Learning Research*, 23:2249–2281, 2022. [1](#)
- [14] Jonathan Ho and Tim Salimans. Classifier-free diffusion guidance. In *NeurIPS 2021 Workshop on Deep Generative Models and Downstream Applications*, 2021. [2](#), [3](#)
- [15] S. Hong, et al. On exact inversion of dpm-solvers. *CVPR*, 2024. [3](#)
- [16] Jiancheng Huang, Yifan Liu, Jiayi Lv, and Shifeng Chen. Entwined inversion: Tune-free inversion for real image faithful reconstruction and editing. In *ICASSP 2024-2024 IEEE International Conference on Acoustics, Speech and Signal Processing (ICASSP)*, pages 2920–2924. IEEE, 2024. [1](#)
- [17] Jiancheng Huang, Yifan Liu, Jin Qin, and Shifeng Chen. Kv inversion: Kv embeddings learning for text-conditioned real image action editing. *arXiv preprint arXiv:2309.16608*, 2023. [1](#)
- [18] Jiancheng Huang, Yifan Liu, Linxiao Shi, Jin Qin, and Shifeng Chen. Bk-editer: Body-keeping text-conditioned real image editing. In *International Conference on Computational Visual Media*, pages 235–251. Springer, 2024. [1](#)
- [19] Jiancheng Huang, Mingfu Yan, Songyan Chen, Yi Huang, and Shifeng Chen. Magicfight: Personalized martial arts combat video generation. In *Proceedings of the 32nd ACM International Conference on Multimedia*, pages 10833–10842, 2024. [1](#)
- [20] Jiancheng Huang, Mingfu Yan, Yifan Liu, and Shifeng Chen. Color-sd: Stable diffusion model already has a color style noisy latent space. In *2024 IEEE International Conference on Multimedia and Expo (ICME)*, pages 1–6. IEEE, 2024. [2](#)
- [21] Jiancheng Huang, Mingfu Yan, Yifan Liu, and Shifeng Chen. Sbr: Stochasticity beats content restriction problem in training and tuning free image editing. In *Proceedings of the 2024 International Conference on Multimedia Retrieval*, pages 878–887, 2024. [1](#)
- [22] Yi Huang, Jiancheng Huang, Jianzhuang Liu, Yu Dong, Jiayi Lv, and Shifeng Chen. Wavedm: Wavelet-based diffusion models for image restoration. *TMM*, 2024. [2](#)
- [23] Yi Huang, Jiancheng Huang, Yifan Liu, Mingfu Yan, Jiayi Lv, Jianzhuang Liu, Wei Xiong, He Zhang, Shifeng Chen, and Liangliang Cao. Diffusion model-based image editing: A survey. *arXiv preprint arXiv:2402.17525*, 2024. [2](#)
- [24] Yuzhou Huang, Liangbin Xie, Xintao Wang, Ziyang Yuan, Xiaodong Cun, Yixiao Ge, Jiantao Zhou, Chao Dong, Rui Huang, Ruimao Zhang, et al. Smartedit: Exploring complex instruction-based image editing with multimodal large language models. In *CVPR*, pages 8362–8371, 2024. [1](#)
- [25] Inbar Huberman-Spiegelglas, Vladimir Kulikov, and Tomer Michaeli. An edit friendly ddp noise space: Inversion and manipulations. In *CVPR*, 2024. [2](#), [7](#)
- [26] Betker James, Goh Gabriel, Jing Li, Brooks Tim, Wang Jianfeng, Li Linjie, Ouyang Long, and et.al. Improving image generation with better captions. *Computer Science*, 2:8, 2023. [2](#)
- [27] Xuan Ju, Ailing Zeng, Yuxuan Bian, Shaoteng Liu, and Qiang Xu. Direct inversion: Boosting diffusion-based editing with 3 lines of code. In *ICLR*, 2024. [6](#), [2](#)
- [28] Bahjat Kawar, Shiran Zada, Oran Lang, Omer Tov, Huiwen Chang, Tali Dekel, Inbar Mosseri, and Michal Irani. Imagic: Text-based real image editing with diffusion models. In *CVPR*, 2023. [1](#)
- [29] Nupur Kumari, Bingliang Zhang, Richard Zhang, Eli Shechtman, and Jun-Yan Zhu. Multi-concept customization of text-to-image diffusion. In *CVPR*, 2023. [1](#), [2](#)
- [30] Junnan Li, Dongxu Li, Caiming Xiong, and Steven Hoi. Blip: Bootstrapping language-image pre-training for unified vision-language understanding and generation. In *ICML*, 2022. [5](#)
- [31] Manling Li, Ruochen Xu, Shuohang Wang, Luwei Zhou, Xudong Lin, Chenguang Zhu, Michael Zeng, Heng Ji, and

- Shih-Fu Chang. Clip-event: Connecting text and images with event structures. In *CVPR*, 2022. 2
- [32] Shanglin Li, Bohan Zeng, Yutang Feng, Sicheng Gao, Xihui Liu, Jiaming Liu, Lin Li, Xu Tang, Yao Hu, Jianzhuang Liu, et al. Zone: Zero-shot instruction-guided local editing. In *CVPR*, pages 6254–6263, 2024. 1
- [33] Chang Liu, Xiangtai Li, and Henghui Ding. Referring image editing: Object-level image editing via referring expressions. In *CVPR*, pages 13128–13138, 2024. 1
- [34] Jiayi Lv, Yi Huang, Mingfu Yan, Jiancheng Huang, Jianzhuang Liu, Yifan Liu, Yafei Wen, Xiaoxin Chen, and Shifeng Chen. Gpt4motion: Scripting physical motions in text-to-video generation via blender-oriented gpt planning. In *Proceedings of the IEEE/CVF Conference on Computer Vision and Pattern Recognition*, pages 1430–1440, 2024. 1
- [35] Chenlin Meng, Yang Song, Jiaming Song, Jiajun Wu, Jun-Yan Zhu, and Stefano Ermon. Sdedit: Image synthesis and editing with stochastic differential equations. In *ICLR*, 2021. 3, 5, 2
- [36] Sewon Min, Xinxi Lyu, Ari Holtzman, Mikel Artetxe, Mike Lewis, Hannaneh Hajishirzi, and Luke Zettlemoyer. Rethinking the role of demonstrations: What makes in-context learning work? In *EMNLP*, 2022. 5
- [37] Daiki Miyake, Akihiro Iohara, Yu Saito, and Toshiyuki Tanaka. Negative-prompt inversion: Fast image inversion for editing with text-guided diffusion models. *arXiv preprint arXiv:2305.16807*, 2023. 1, 2, 3, 6, 7
- [38] Ron Mokady, Amir Hertz, Kfir Aberman, Yael Pritch, and Daniel Cohen-Or. Null-text inversion for editing real images using guided diffusion models. In *CVPR*, 2023. 1, 2, 3, 6, 7
- [39] Hyelin Nam, Gihyun Kwon, Geon Yeong Park, and Jong Chul Ye. Contrastive denoising score for text-guided latent diffusion image editing. In *CVPR*, pages 9192–9201, 2024. 1
- [40] Jisu Nam, Heesu Kim, DongJae Lee, Siyoon Jin, Seungryong Kim, and Seunggyu Chang. Dreammatcher: Appearance matching self-attention for semantically-consistent text-to-image personalization. In *CVPR*, pages 8100–8110, 2024. 1
- [41] Alex Nichol, Prafulla Dhariwal, Aditya Ramesh, Pranav Shyam, Pamela Mishkin, Bob McGrew, Ilya Sutskever, and Mark Chen. Glide: Towards photorealistic image generation and editing with text-guided diffusion models. In *ICML*, 2022. 1, 2
- [42] Z. Pan, et al. Effective real image editing with accelerated iterative diffusion inversion. In *ICCV*, 2023. 3, 2
- [43] Gaurav Parmar, Krishna Kumar Singh, Richard Zhang, Yijun Li, Jingwan Lu, and Jun-Yan Zhu. Zero-shot image-to-image translation. In *ACM SIGGRAPH*, 2023. 1
- [44] Aditya Ramesh, Prafulla Dhariwal, Alex Nichol, Casey Chu, and Mark Chen. Hierarchical text-conditional image generation with clip latents. *arXiv preprint arXiv:2204.06125*, 2022. 1, 2
- [45] Robin Rombach, Andreas Blattmann, Dominik Lorenz, Patrick Esser, and Björn Ommer. High-resolution image synthesis with latent diffusion models. In *CVPR*, 2022. 1, 2, 3, 6
- [46] Nataniel Ruiz, Yuanzhen Li, Varun Jampani, Yael Pritch, Michael Rubinstein, and Kfir Aberman. Dreambooth: Fine tuning text-to-image diffusion models for subject-driven generation. In *CVPR*, 2023. 1, 2, 7
- [47] Chitwan Saharia, William Chan, Saurabh Saxena, Lala Li, Jay Whang, Emily Denton, Seyed Kamyar Seyed Ghasemipour, Burcu Karagol Ayan, S Sara Mahdavi, Rapha Gontijo Lopes, et al. Photorealistic text-to-image diffusion models with deep language understanding. In *NeurIPS*, 2022. 2, 3
- [48] Jascha Sohl-Dickstein, Eric Weiss, Niru Maheswaranathan, and Surya Ganguli. Deep unsupervised learning using nonequilibrium thermodynamics. In *ICML*, 2015. 2
- [49] Jiaming Song, Chenlin Meng, and Stefano Ermon. Denoising diffusion implicit models. In *ICLR*, 2020. 1, 2, 3, 6
- [50] Xue Song, Jiequan Cui, Hanwang Zhang, Jingjing Chen, Richang Hong, and Yu-Gang Jiang. Doubly abductive counterfactual inference for text-based image editing. In *CVPR*, pages 9162–9171, 2024. 1
- [51] Yang Song and Stefano Ermon. Generative modeling by estimating gradients of the data distribution. In *NeurIPS*, 2019. 1, 2
- [52] Narek Tumanyan, Michal Geyer, Shai Bagon, and Tali Dekel. Plug-and-play diffusion features for text-driven image-to-image translation. In *CVPR*, 2023. 1, 2, 3
- [53] B. Wallace, et al. Edict: Exact diffusion inversion via coupled transformations. In *CVPR*, 2023. 2, 3
- [54] Yuxiang Wei, Yabo Zhang, Zhilong Ji, Jinfeng Bai, Lei Zhang, and Wangmeng Zuo. Elite: Encoding visual concepts into textual embeddings for customized text-to-image generation. In *ICCV*, 2023. 1, 2, 6, 7, 8
- [55] Guangxuan Xiao, Tianwei Yin, William T Freeman, Frédo Durand, and Song Han. Fastcomposer: Tuning-free multi-subject image generation with localized attention. *arXiv preprint arXiv:2305.10431*, 2023. 1, 2
- [56] Jiahui Yu, Yuanzhong Xu, Jing Yu Koh, Thang Luong, Guntjan Baid, Zirui Wang, Vijay Vasudevan, Alexander Ku, Yinfei Yang, Burcu Karagol Ayan, et al. Scaling autoregressive models for content-rich text-to-image generation. *Transactions on Machine Learning Research*, 2022. 1, 2
- [57] Richard Zhang, Phillip Isola, Alexei A Efros, Eli Shechtman, and Oliver Wang. The unreasonable effectiveness of deep features as a perceptual metric. In *CVPR*, 2018. 8
- [58] Donghao Zhou, Jiancheng Huang, Jinbin Bai, Jiaye Wang, Hao Chen, Guangyong Chen, Xiaowei Hu, and Pheng-Ann Heng. Magictailor: Component-controllable personalization in text-to-image diffusion models. *arXiv preprint arXiv:2410.13370*, 2024. 2

GPT-4 Synthetic Training Text Dataset



“I want to make 10000 triple samples.”

You are an expert in English writing. Please generate 10000 triple samples for me, each sample comprising a source text, a target text, and an associated editing task label. We classify text-conditional image editing into five categories: 1) Object Replacement: Replacing an object in the image with another object; 2) Action Editing: Preserving the background and the object identity but altering his/her/its action; 3) Scene Editing: Keeping the objects in the image unchanged while transforming the scene; 4) Object Adding: Adding a new object to the image while keeping the unedited part of the image unchanged; 5) Style Editing: Modifying the artistic style of the image. I show you some samples of these five categories:

Source: A snowy landscape with a lone pine tree.
Target: A snowy landscape with a tower.
Task: Object Replacement

Source: A dog sleeping in a sunny spot on the carpet.
Target: A dog playing with a ball in a sunny spot on the carpet.
Task: Action Editing

Source: A burger on a plate.
Target: A burger and a tomato on the plate.
Task: Object Adding

Source: A small boat on a calm lake at noon.
Target: A small boat on a calm lake under a starry night sky.
Task: Scene Editing

Source: A digital art portrait of a woman.
Target: An impressionist-style painting of the same woman.
Task: Style Editing



Here are the 10000 samples:

- Source: A black cat sitting on a blue sofa.
- Target: A yellow tiger sitting on a blue sofa.
- Task: Object Replacement

- Source: A man standing in a park holding a frisbee.
- Target: A man running in the park.
- Task: Action Editing

- Source: A woman baking bread in a bright kitchen.
- Target: A woman baking bread in the forest.
- Task: Scene Editing

- Source: A child playing soccer on an empty grass field.
- Target: A child and his dog playing soccer on the grass field.
- Task: Object Adding

- Source: A watercolor painting depicting a countryside landscape.
- Target: An oil painting style artwork of a countryside landscape.
- Task: Style Editing

- Source: A laptop open on a desk next to a coffee cup.
- Target: A notebook open on a desk next to a coffee cup.
- Task: Object Replacement

- Source: A bear standing on the grass.
- Target: A bear jumping on the grass.
- Task: Action Editing

.....

Figure S10. Using GPT4 to generate our triple dataset.

In this supplementary material, we (1) show how to build the training dataset for the editing task classifier and the structure of the classifier, (2) give more ablation study, (3) show all the test images with prompts, (4) prove \bar{z}_1^p and \bar{z}_{10}^a obtained by DDIM does not affect our reversibility, (5) provide more reconstruction examples across different CFG scales, and (6) summarize recent inversion and editing methods in Table S8.

A. Editing Tasks Classification

In the main paper, we classify text-conditional image editing into five categories: 1) *Object Replacement*: Replacing an object in the image with another object; 2) *Action Editing*: Preserving the background and the object identity but altering his/her/its action; 3) *Scene Editing*: Keeping the objects in the image unchanged while transforming the scene; 4) *Object Adding*: Adding a new object to the image while keeping the unedited part of the image unchanged; 5) *Style Editing*: Modifying the artistic style of the image. We first utilize GPT-4 to generate a substantial training dataset

Network	Setting	Value
Classifier	Input Channel	768
	Token Number	154 (77 × 2)
	Transformer block channels	512
	Attention head number	8
	Residual Connection	True
	Block numbers	6
	Final linear layer input channels	512
	Final linear layer output channels	5

Table S7. Model configurations and parameter choices.

of triple samples as shown in Fig. S10, each comprising a source text, a target text, and an associated editing task label. We give some examples of our dataset in Fig. S11.

Subsequently, leveraging the text embeddings extracted by the CLIP text encoder, we design a Transformer-based editing task classifier as shown in Table S7. This classifier takes as input the concatenated embeddings of the source and target texts. After processing through multiple Transformer blocks, a classification head at the final layer outputs

Task Label	Object Replacement	Action Editing	Scene Editing	Object Adding	Style Editing
Source Text	A black cat sitting on a blue sofa.	A man standing in a park holding a frisbee.	A woman baking bread in a bright kitchen.	A child playing soccer on an empty grass field.	A watercolor painting depicting a countryside landscape.
Target Text	An orange dog sitting on a blue sofa.	A man running in the park.	A woman baking bread in a bedroom.	A child and his dog playing soccer on the grass field.	An oil painting style artwork of a countryside landscape.
Source Text	A red sports car parked in a parking lot.	A chef cutting onions in the kitchen.	An astronaut floating inside a space station.	A girl walking alone on the beach.	A photo of a forest in real life.
Target Text	A tank parked in a parking lot.	A chef stirring soup in the kitchen.	An astronaut floating in a space station with an alien landscape view.	A girl and a seagull walking on the beach.	An impressionist style painting of a forest.

Figure S11. Examples of our triple dataset.

Type	Learning Strategy	Method
Inversion	Testing-Time Finetuning	Null-Text Inversion [38] Textual Inversion [6] AIDI [42]
	Training & Tuning Free	DDIM Inversion [49] DDPM Inversion [25] N-P Inversion [37] ProxEdit [9] EDICT [53] NMG [4] DirectInv [27] Dual-Schedule Inversion
Editing	Training-Based	ELITE [54] FastComposer [55] InstructPix2Pix [2]
	Testing-Time Finetuning	DreamBooth [46] Custom Diffusion [29]
	Training & Tuning Free	SDEdit [35] P2P [10] MasaCtrl [3]

Table S8. Some recent inversion and editing methods. N-P Inversion denotes Negative-Prompt Inversion [37].

the predicted editing task category.

B. Results of Ablation Study on Auxiliary Schedules

As mentioned in Sec. 5.3, the reconstruction performances are very similar in three settings of τ . However, when $\tau = t - s + \frac{1}{4}s$ or $\tau = t - s + \frac{3}{4}s$, the editing performances are not as good as when $\tau = t - s + \frac{s}{2}$. For instance, we give a scene editing example in Fig. S12. It can be seen that slight blurring, artifacts, and strange textures may be present in certain regions of the edited image when $\tau = t - s + \frac{1}{4}s$ or $\tau = t - s + \frac{3}{4}s$.

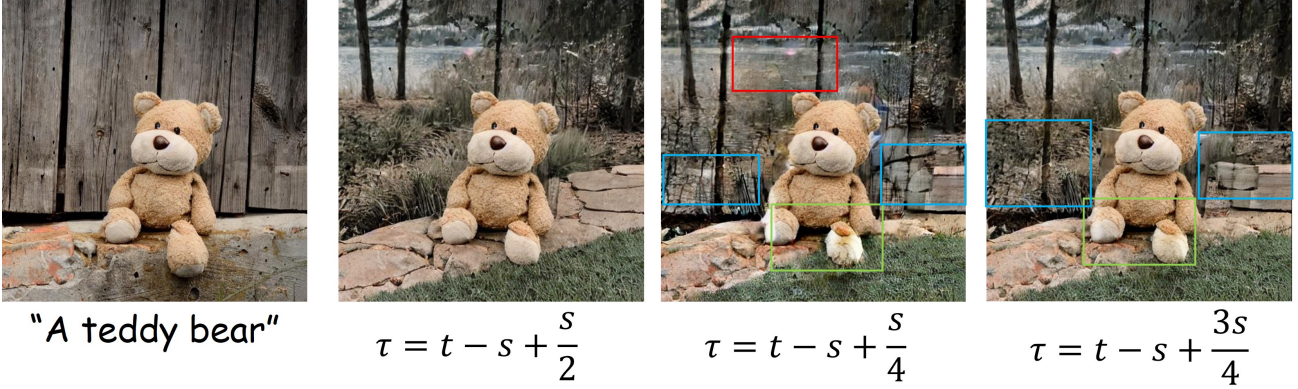
C. Testing Dataset

Due to the lack of public benchmarks for the evaluation, we build a testing set in this work. The set has a total of 150 image-text pairs, among which 32 pairs are from all the examples used by three related works^{4,5,6} [2, 3, 54], and the rest of 118 pairs are from the Internet. All images are interpolated, cut, and/or scaled to the size of 512×512 . We use all the images for the reconstruction experiment and the first 20 images for the editing experiment. The complete set of the image-text pairs is presented in Figs. S13, S14, S15, and S16.

⁴timothybrooks.com/instruct-pix2pix

⁵<https://ljzycmd.github.io/projects/MasaCtrl>

⁶<https://github.com/csyxwei/ELITE>



"A teddy bear near the tree and grass"

Figure S12. Editing results with $\tau = t - s + \frac{s}{2}$, $\tau = t - s + \frac{s}{4}$, or $\tau = t - s + \frac{3s}{4}$. Slight blurring (red boxes), artifacts (green boxes), and strange textures (blue boxes) appear in the last two edited images.

D. Initial Latent Setup and Reversibility Proof

In Section 4.2 of the main paper, we state that \bar{z}_1^p and \bar{z}_{10}^a obtained by the original forward process of DDIM do not affect our method’s reversibility. To prove it, we need to ensure that these initial values conform to the conditions required for reversibility.

Mathematically, given \bar{z}_1^p and \bar{z}_{10}^a obtained by DDIM, we need to prove:

$$\bar{z}_1^p = \bar{z}_1^p, \quad (15)$$

which represents the reversibility of our inversion and sampling since \bar{z}_1^p and \bar{z}_1^p denote the beginning of the inversion stage and the endpoint of the sampling stage, respectively.

Proposition 1. *Let \bar{z}_1^p and \bar{z}_{10}^a be obtained by the original forward process of DDIM. Then $\bar{z}_1^p = \bar{z}_1^p$ where \bar{z}_1^p is obtained by the Dual-Schedule Inversion method presented in Section 4.3 of the main paper.*

Proof. Given \bar{z}_1^p and \bar{z}_{10}^a , we can obtain \bar{z}_{21}^p using Eq. 11:

$$\bar{z}_{21}^p = a_{(1 \rightarrow 21)} \bar{z}_1^p + b_{(1 \rightarrow 21)} \epsilon_{\theta}(\bar{z}_{10}^a, 10). \quad (16)$$

Similarly, given \bar{z}_{21}^p and \bar{z}_{10}^a , we can obtain \bar{z}_{30}^a using Eq. 12:

$$\bar{z}_{30}^a = a_{(10 \rightarrow 30)} \bar{z}_{10}^a + b_{(10 \rightarrow 30)} \epsilon_{\theta}(\bar{z}_{21}^p, 21). \quad (17)$$

By iterating this inversion process, we ultimately obtain:

$$\bar{z}_{981}^p = a_{(961 \rightarrow 981)} \bar{z}_{961}^p + b_{(961 \rightarrow 981)} \epsilon_{\theta}(\bar{z}_{970}^a, 970). \quad (18)$$

From the Reversibility Requirement part in Section 4.2, the sampling process from $t = 981$ is reversible in the inversion process. Thus, at time steps $t = 30$ and $\tau = 21$ during the sampling stage, we have $\bar{z}_{30}^a = \bar{z}_{30}^a$ and $\bar{z}_{21}^p = \bar{z}_{21}^p$. Given \bar{z}_{21}^p and \bar{z}_{30}^a , we can compute:

$$\bar{z}_{10}^a = a_{(30 \rightarrow 10)} \bar{z}_{30}^a + b_{(30 \rightarrow 10)} \epsilon_{\theta}(\bar{z}_{21}^p, 21). \quad (19)$$

Comparing Eq. 19 with Eq. 17, we have $\bar{z}_{10}^a = \bar{z}_{10}^a$ since these two equations are actually the same.

Finally, given \bar{z}_{10}^a and \bar{z}_{21}^p , we obtain:

$$\bar{z}_1^p = a_{(21 \rightarrow 1)} \bar{z}_{21}^p + b_{(21 \rightarrow 1)} \epsilon_{\theta}(\bar{z}_{10}^a, 10). \quad (20)$$

Again, comparing Eq. 20 with Eq. 16, we have $\bar{z}_1^p = \bar{z}_1^p$, which completes the proof. \square

E. More Reconstruction Examples

Here we provide 10 reconstruction examples across different guidance scales 1, 4, and 7.5 in Fig. S17, S18, and S19.



"A red chair"



"Two bikers in the city"



"A lake"



"A statue"



"A man"



"A ball"



"A dog"



"Two cars"



"A car"



"A fountain"



"A biker"



"A mountain"



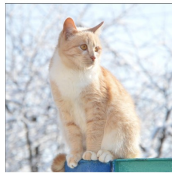
"A pushchair"



"A camel"



"A lake"



"A cat"



"A cat"



"An elephant"



"Two dog"



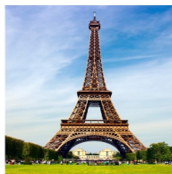
"A vase of flowers"



"A horse is running"



"Sun flowers"



"Paris Tower"



"Man with fruit"



"Toy Story"



"A lake"



"Planting"



"4 mans in the street"



"Mona Lisa"



"Lake of city"



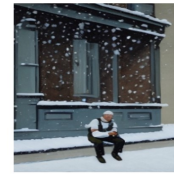
"A painting of flowers"



"Pairs Tower"



"A man with cake"



"A man in winter"



"A cowboy"



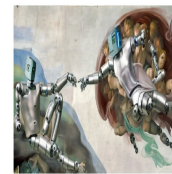
"A man"



"A lake"



"A city"



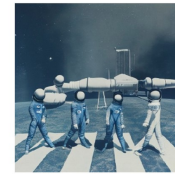
"Two robotics"



"Italy city"



"Night street"



"Aliens"

Figure S13. Images of the testing dataset (Part 1).

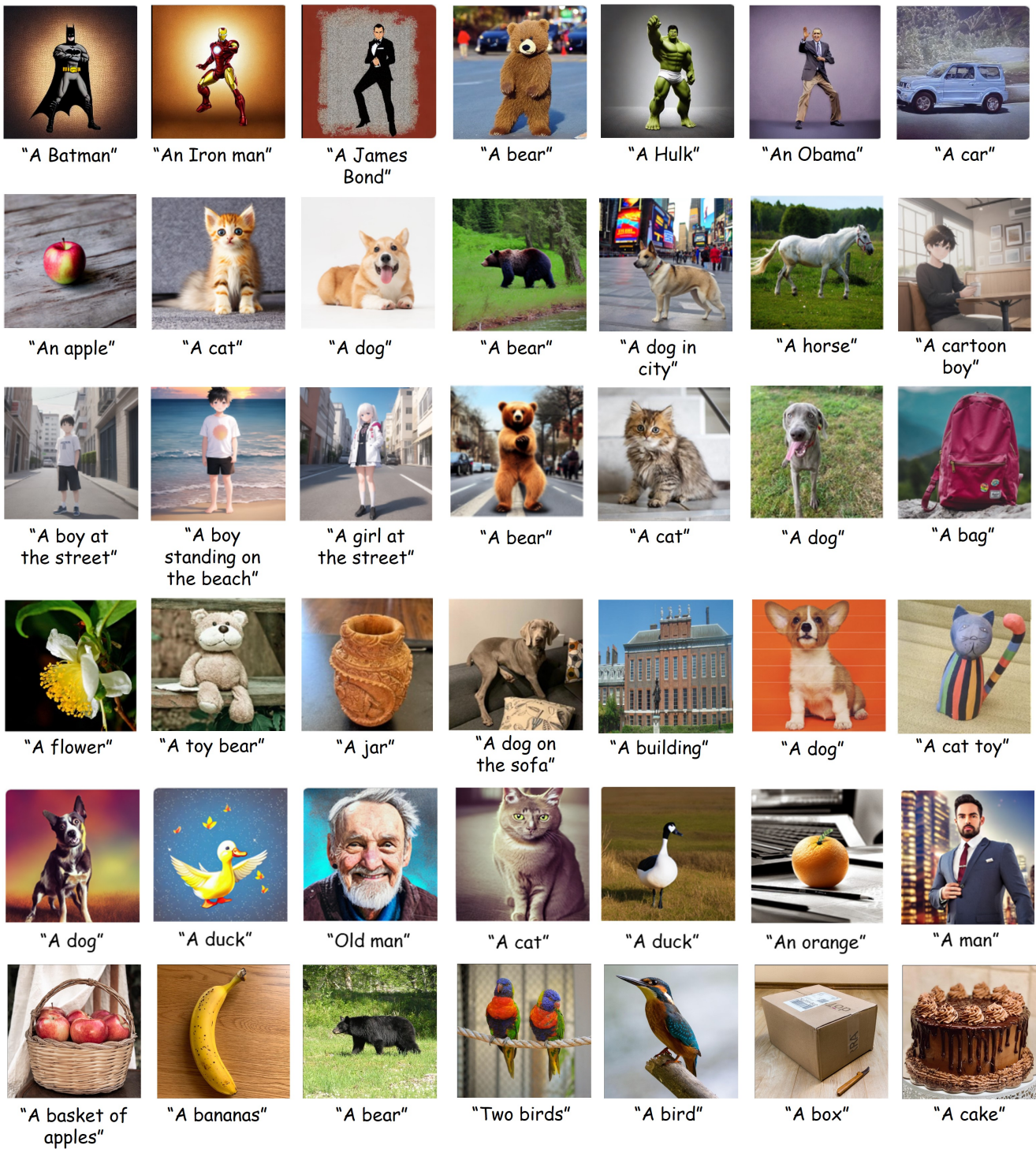


Figure S14. Images of the testing dataset (Part 2).

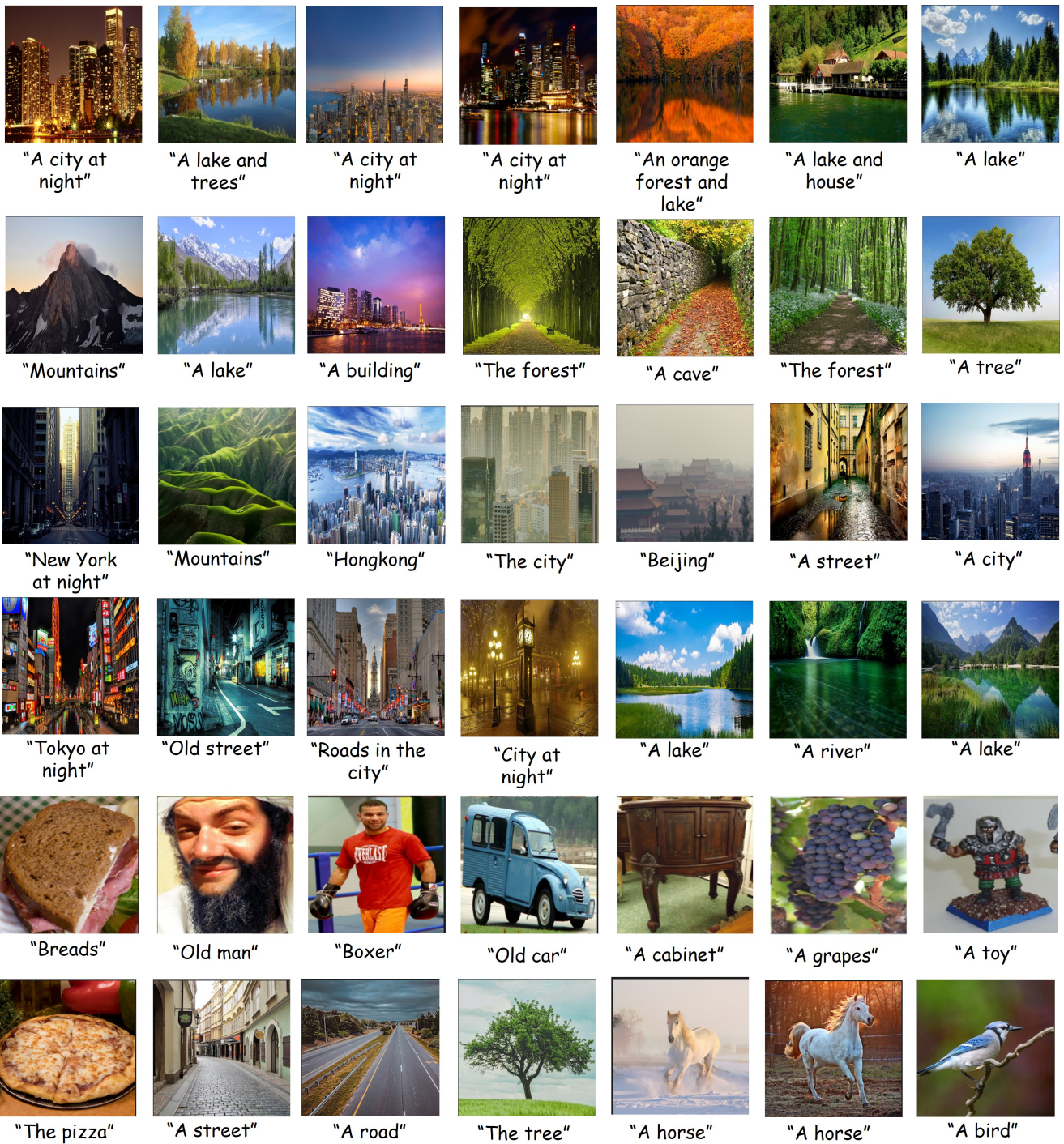


Figure S15. Images of the testing dataset (Part 3).

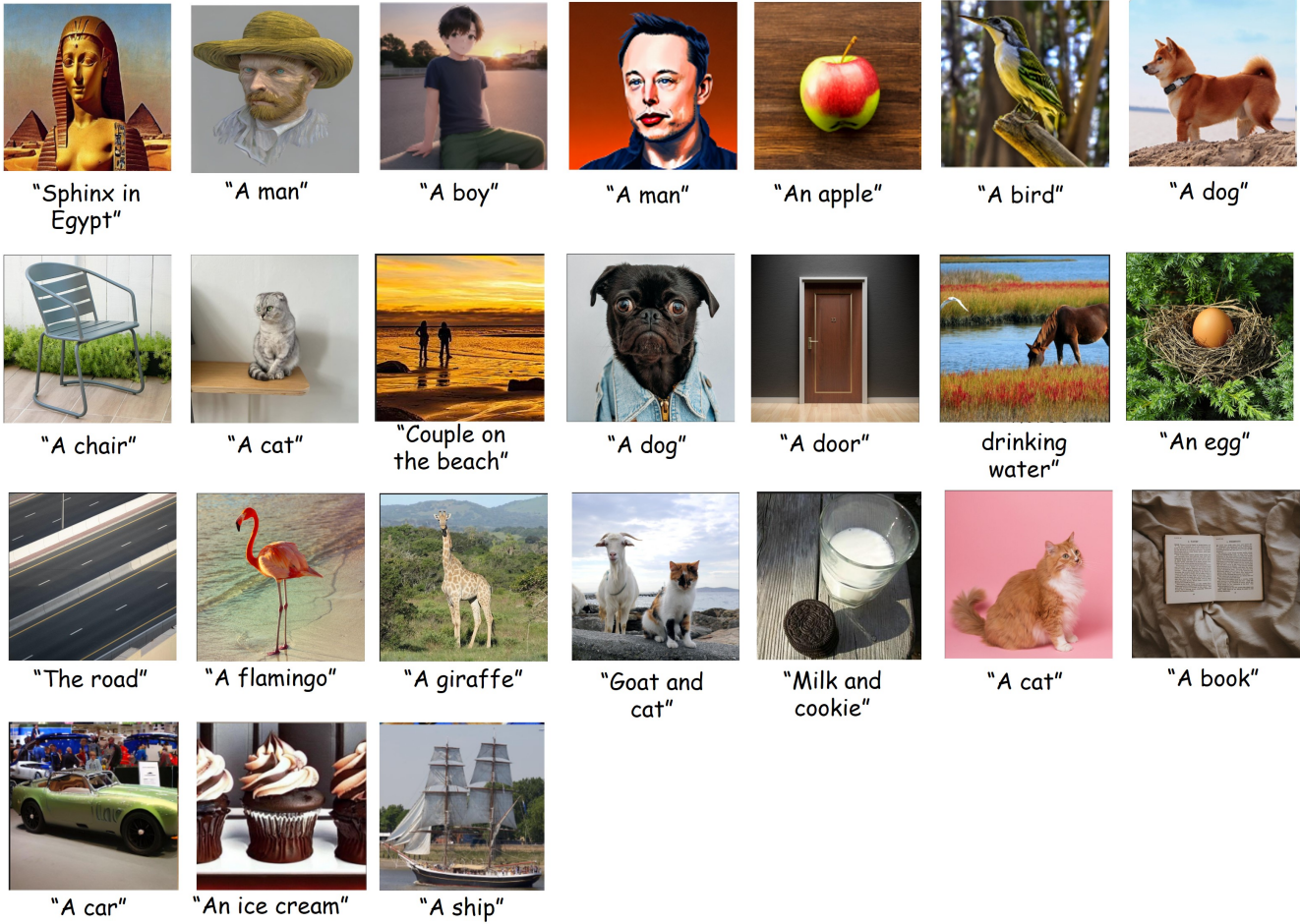


Figure S16. Images of the testing dataset (*Part 4*).

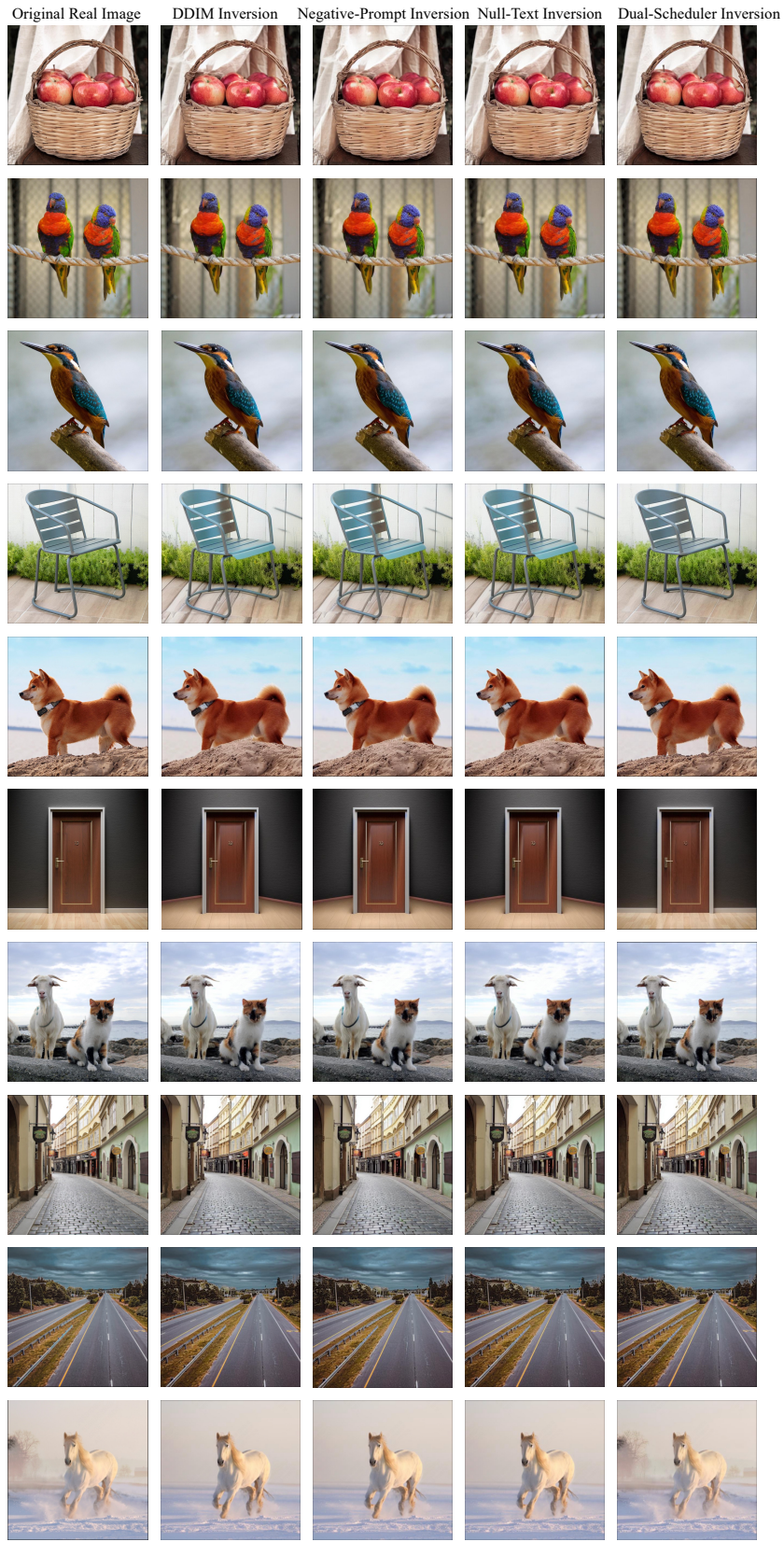


Figure S17. Reconstruction examples (*guidance scale* $w = 1$). While Null-Text Inversion requires fine-tuning, the other three methods do not. Dual-Schedule Inversion achieves excellent performance without fine-tuning.

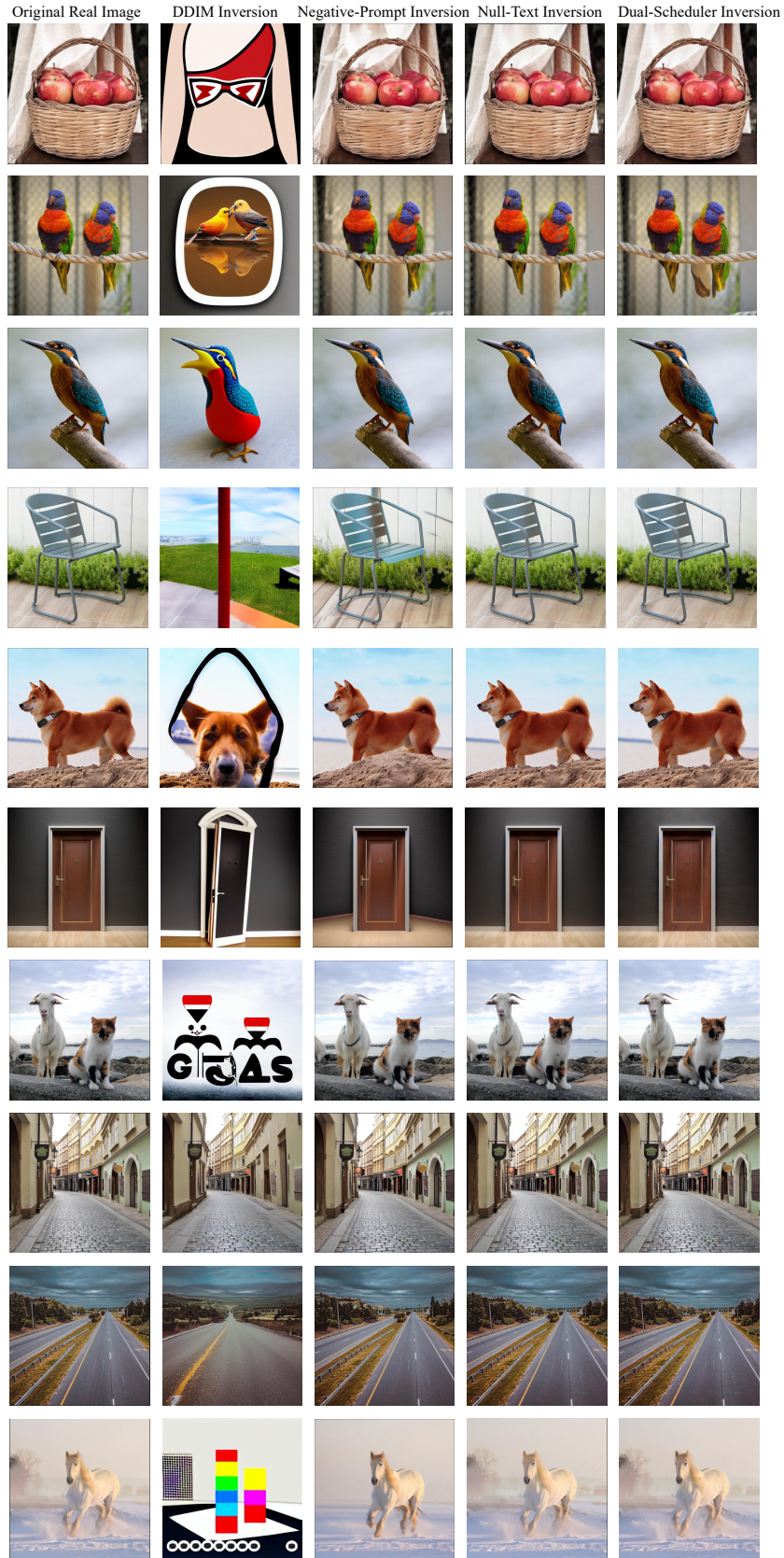


Figure S18. Reconstruction examples (*guidance scale* $w = 4$). While Null-Text Inversion requires fine-tuning, the other three methods do not. Dual-Schedule Inversion achieves excellent performance without fine-tuning.

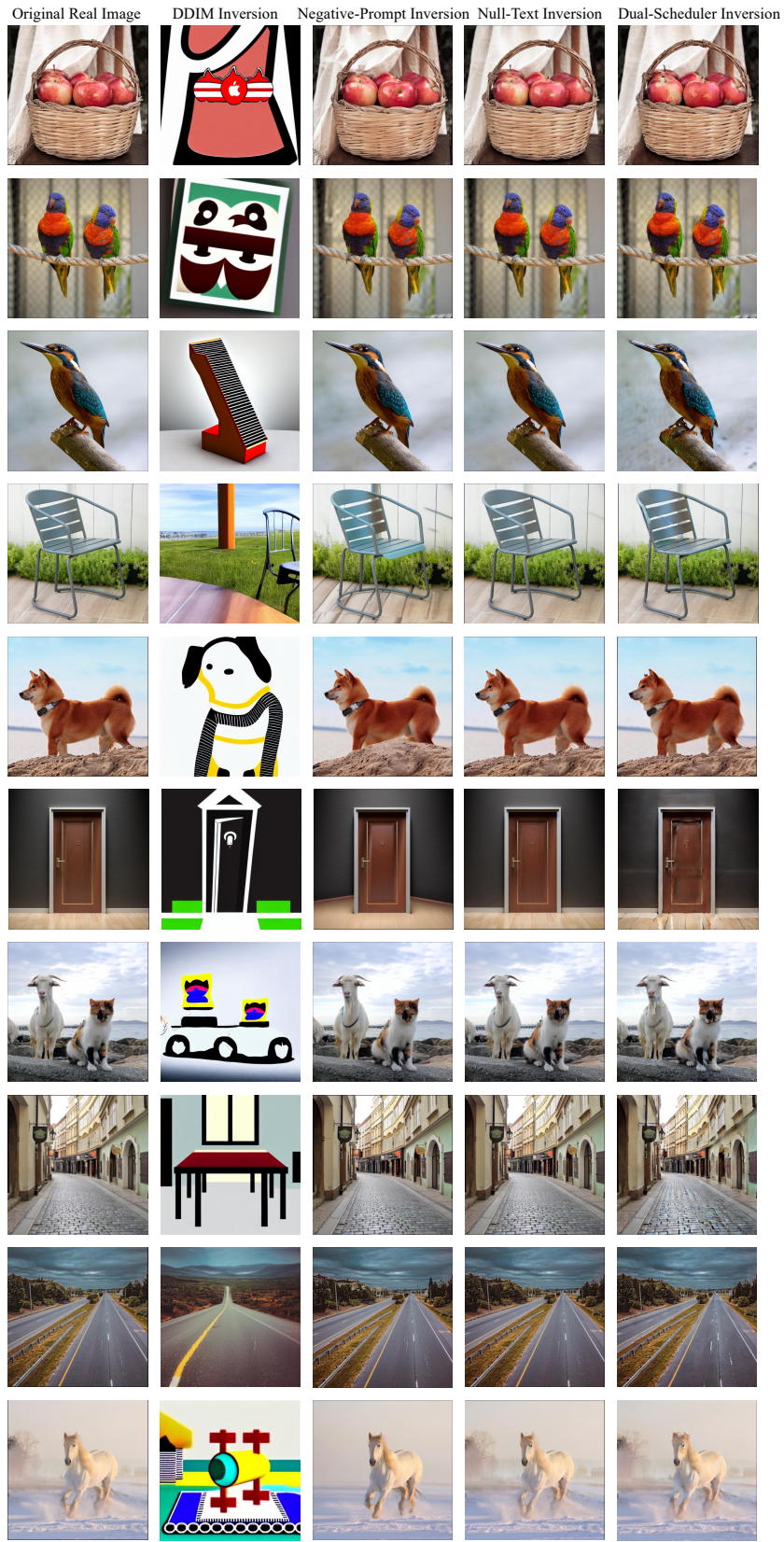


Figure S19. Reconstruction examples (*guidance scale* $w = 7.5$). While Null-Text Inversion requires fine-tuning, the other three methods do not. Dual-Schedule Inversion achieves excellent performance without fine-tuning.